Development 133, 4035-4044 (2006) doi:10.1242/dev.02580

At the next stop sign turn right: the metalloprotease Tolloid-related 1 controls defasciculation of motor axons in *Drosophila*

Frauke Meyer and Hermann Aberle*

Navigation of motoneuronal growth cones toward the somatic musculature in *Drosophila* serves as a model system to unravel the molecular mechanisms of axon guidance and target selection. In a large-scale mutagenesis screen, we identified *piranha*, a motor axon guidance mutant that shows strong defects in the neuromuscular connectivity pattern. In *piranha* mutant embryos, permanent defasciculation errors occur at specific choice points in all motor pathways. Positional cloning of *piranha* revealed point mutations in *tolloid-related 1* (*tlr1*), an evolutionarily conserved gene encoding a secreted metalloprotease. Ectopic expression of Tlr1 in several tissues of *piranha* mutants, including hemocytes, completely restores the wild-type innervation pattern, indicating that Tlr1 functions cell non-autonomously. We further show that loss-of-function mutants of related metalloproteases do not have motor axon guidance defects and that the respective proteins cannot functionally replace Tlr1. *tlr1*, however, interacts with *sidestep*, a muscle-derived attractant. Double mutant larvae of *tlr1* and *sidestep* show an additive phenotype and lack almost all neuromuscular junctions on ventral muscles, suggesting that Tlr1 functions together with Sidestep in the defasciculation process.

KEY WORDS: *Drosophila*, Neuromuscular junction, Motor axon guidance, Motoneuron, Metalloprotease, Tolloid, Tolkin, Tolloid-related 1, Sidestep, Kuzbanian

INTRODUCTION

Accurate innervation of somatic muscles is a prerequisite for coordinated movements in any higher organism. During embryogenesis, correct neuromuscular connectivity is established by the developmental processes of axon outgrowth, axon guidance, target selection and synapse formation (Tessier-Lavigne and Goodman, 1996). Despite the fact that motor axons initially form coherent nerve bundles, certain growth cones leave these tightly fasciculated nerves at specific peripheral locations in order to migrate into their target regions. Defasciculation, the exit of axons from a nerve track, is therefore a crucial process that needs to be strictly regulated. Failure to defasciculate at these choice points leads to axon guidance defects and muscle innervation errors (Araujo and Tear, 2003). Which molecules regulate the detachment of motor axons from adherent nerve bundles? How are choice points molecularly defined?

The *Drosophila* neuromuscular innervation pattern provides a powerful experimental system to genetically dissect the molecular mechanisms of defasciculation and motor axon guidance in vivo. Trajectories of motor axons and their branching patterns are stereotypic and segmentally repeated (Sink and Whitington, 1991), as are the positions of neuromuscular terminals on muscle fibers (Hoang and Chiba, 2001). This relatively simple anatomy, together with the available genetic tools in *Drosophila*, have been of great advantage to identify genes and gene families with roles in motor axon guidance, including the Semaphorins (Kolodkin et al., 1993) and Netrins (Mitchell et al., 1996). Furthermore, three molecules have been identified that seem to specifically control defasciculation of motor axons: the transmembrane tyrosine phosphatase Lar (leukocyte common antigen-related) and the members of the immunoglobulin superfamily Beaten path (Beat) and Sidestep (Side), all three of which give rise to highly penetrant motor axon guidance phenotypes (Desai et al., 1996; Fambrough and Goodman, 1996; Krueger et al., 1996; Sink et al., 2001). Sidestep is expressed in somatic muscles during the period of motor axon pathfinding and is thought to function as a muscle-derived attractant for motor nerves (Sink et al., 2001). In *sidestep* mutant embryos, motor axons frequently bypass their targets, as they fail to defasciculate from their nerve tracts. As Lar, Beat and Side give rise to similar bypass phenotypes when mutated, they all seem to be involved in the defasciculation process, but how they interact mechanistically, and whether additional regulators are required, is currently unknown.

Here, we describe *piranha*, a novel axon guidance mutant with defasciculation defects. In *piranha* mutants, we identified point mutations in the evolutionarily conserved gene *tolloid-related 1* (*tlr1*), also called *tolkin* (*tok*), which encodes an extracellular metalloprotease (Nguyen et al., 1994; Finelli et al., 1995). Mutations in *tlr1*, but not in related *Drosophila* metalloproteases, lead to stable innervation errors that persist into larval stages. Motor nerves stay attached to each other at places where they should diverge and consequently fail to reach their muscle targets or use irregular routes. Genetic rescue experiments demonstrate that Tlr1 functions non-cell-autonomously, possibly in the hemolymph. In addition, the proteolytic activity of Tlr1 is required in cooperation with other axon guidance molecules, such as Sidestep, to terminate coherent axon-axon interactions at choice points.

Max-Planck-Institute for Developmental Biology, Department III/Genetics, Spemannstrasse 35, 72076 Tübingen, Germany.

*Author for correspondence (e-mail: hermann.aberle@tuebingen.mpg.de)

Accepted 10 August 2006

MATERIALS AND METHODS

Genetics and fly stocks

The mutant alleles of *tlr1* ($tlr1^{D427}$, $tlr1^{I678}$, $tlr1^{K598}$ and $tlr1^{K788}$) and *side* ($side^{C137}$, $side^{I306}$, $side^{I1563}$, $side^{K717}$) were isolated in an F2 methanesulfonic acid ethylester (EMS)-mutagenesis screen on the third chromosome for

recessive mutations affecting the structure of neuromuscular junctions (NMJs) (Aberle et al., 2002). The *side, tlr1* double mutants were constructed by recombination using recessive markers of the rucuca-chromosome. *UAS-tlr1* and *UAS-tld*^{23A} were a kind gift of Michael O'Connor. The *tolloid* alleles *tld*^{10E95}, *tld*^{9B66}, *tld*^{6B69} and *tld*^{7074} and Heat shock-Gal4 were provided by the Tübingen stock collection. *tlr1*^{1}, *tlr1*^{3}, *kuz*^{E29}, *kuz*^{K01403}, *Mmp1*^{k04809}, *Mmp2*^{k00604} and *Mmp2*^{KG01263}, *UAS-kuz*^{F}, *UAS-dsRed2* (#6282) and CG-Gal4 were obtained from the Bloomington Stock Center (http://flystocks.bio.indiana.edu/). To assess neuromuscular phenotypes, mutants were crossed into the CD8-GFP-Sh background (Zito et al., 1999). The following Gal4-lines were used: Elav-Gal4, 24B-Gal4 (gifts of C. S. Goodman), G14-Gal4 (Aberle et al., 2002), Cha-Gal4 (Salvaterra and Kitamoto, 2001), Serpent-Gal4 (gift of R. Reuter), PPL-Gal4 (gift of M.J. Pankratz) and OK371-Gal4 (Mahr and Aberle, 2006). As wild-type control strains, y w^{1} or w;; CD8-GFP-Sh were used. Genotypes of larvae with transgenically labeled NMJs and motor nerves were OK371-Gal4/+; CD8-GFP-Sh,UAS-*dsRed2*/+ and OK371-Gal4/+; *tlr1*^{K788}/*tlr1*^{D427},UAS-*dsRed2*. Rescue crosses were performed according to the following scheme: *UAS-GeneX*; *tlr1*^{D427}/TM6B crossed to Tissue-specific-Gal4; *tlr1*^{K788}/TM6B. For heat shock experiments, flies were allowed to lay eggs into the food of their vials for 3 hours. Embryos were then stored for 3, 6 or 9 hours or overnight at room temperature before a heat shock (1 hour, 37°C water bath) was applied.

Complementation and mapping

Mutant lines with similar phenotypes were crossed to each other and judged for non-complementation by the presence of mislocalized NMJs. Mutations were mapped by meiotic recombination against the multiply marked rucuca-chromosome (Bloomington). Mapping was refined using available deficiencies. Df(3R)crb87-4, Df(3R)crb-F89-4 and Df(3R)96B did complement but Df(3R)crb87-5, Df(3R)slo3, Df(3R)XS and Df(3R)XTA1 failed to complement *tlr1* mutations. Database searches were performed at FlyBase (http://flybase.bio.indiana.edu/) and NCBI (http://www.ncbi.nlm.nih.gov/).

Quantification of axon guidance phenotypes

The innervation phenotypes were quantified in intact third instar CD8-GFP-Sh larvae. The locations of NMJs were evaluated through the translucent cuticle in abdominal segments A2-A7 using confocal microscopy. Embryonic guidance phenotypes were quantified in dissected embryos stained with anti-Fas II.

Molecular analysis

Genomic DNA of the *tlr1* alleles was isolated using the QIAamp DNA Mini Kit (Qiagen), amplified by PCR and sequenced on both strands with the BigDye Terminator kit (PE Applied Biosystems). Sequences were analyzed using the Lasergene software package (DNAStar). The partial *tlr1* cDNA clone RH04849 was obtained from BDGP (http://www.fruitfly.org/). Digoxigenin-labeled sense and antisense probes for in situ hybridizations were synthesized from RH04849 (Tautz and Pfeifle, 1989). In situ hybridizations were imaged with an Axiophot light microscope (Zeiss) equipped with a CCD-camera (ProgRes3012).

Immunohistochemistry

Embryos were stained as described (Mahr and Aberle, 2006), except that fluorescent labeling was performed with the TSA Cyanine-3 System (Perkin Elmer). Stained embryos were dissected with sharpened tungsten needles on microscope slides and imaged with an LSM510 confocal microscope (Zeiss) in the Cy3- and DIC channels. Signals in the Cy3-channel were depicted in black to enhance the contrast in overlays with the DIC images. Wandering third instar larvae were dissected in PBS on Sylgaard plates (Dow Corning Corporation) using spring scissors (Fine Science Tools) and insect pins (Emil Arlt). Larval fillets were fixed in 3.7% formaldehyde/PBS for 15 minutes, washed with PTx (PBS containing 0.1% Triton X-100) and blocked in PTx/5% normal goat serum. Primary antibodies were added overnight at 4°C. Fillets were washed with PTx and incubated with fluorescence-labeled secondary antibodies for 1 hour. Stained fillets were cleared in 70% glycerol/PBS and mounted onto microscope slides. The dilutions of the primary antibodies (supernatants) were as follows: mouse anti-Discs large (4F3) 1:100 and mouse anti-Fasciclin II (1D4) 1:5 (gifts of C. S. Goodman). The Cy3-conjugated secondary antibodies were diluted 1:400 (Molecular Probes or Jackson ImmunoResearch). Fluorescently-labeled larvae were examined with a TCS SPL (Leica) or LSM510 (Zeiss) confocal laser scanning microscope. Projections and single images were adjusted for brightness and contrast using Adobe Photoshop.

RESULTS

Piranha mutant larvae display a high degree of missing and mislocalized NMJs

In *Drosophila* embryos and larvae, the somatic musculature of abdominal segments A2-A7 consists of 30 muscles that are individually identifiable and innervated at invariant positions (Fig. 1A). Wiring of the neuromuscular system starts at stage 13 of embryogenesis, when motor axons begin to migrate toward the differentiating muscle fields (van Vactor et al., 1993). In each abdominal hemisegment, two major motor nerves defasciculate into five nerve branches (Fig. 1A). The segmental nerve (SN) bifurcates into the SNa and SNc, and the intersegmental nerve gives rise to a dorsal branch (ISN) and two ventral branches (ISNb and ISNd).

In a large-scale mutagenesis screen for genes that affect the structure and maintenance of NMJs (Parnas et al., 2001; Aberle et al., 2002), we discovered four alleles of a novel mutant, *piranha*, which showed missing and/or mislocalized NMJs. To visualize NMJs in *piranha* mutants, we used the transgenically encoded fusion protein CD8-GFP-Sh (Zito et al., 1999). CD8-GFP-Sh is controlled by a muscle-specific promotor and consists of the extracellular and transmembrane domain of human CD8, fused cytoplasmatically to GFP and a C-terminal domain of the Shaker potassium channel. It binds to the postsynaptic protein Discs large (Dlg) and highlights all NMJs consisting of type Ib and Is boutons (Zito et al., 1999). Using this synaptic marker, we could evaluate NMJs through the translucent cuticle of intact third instar larvae.

In wild-type larvae, the dorsalmost NMJs on muscle pairs 1/9 and 2/10 are normally arranged symmetrically relative to the axis of the ISN (Fig. 1A-C). In *piranha*^{D427}/*piranha*^{K788} mutants, however, we found that muscles 1 and 9 either lacked NMJs completely or were innervated at ectopic sites in 38.1% (muscle 1) or 25.0% (muscle 9) of hemisegments (Table 1, Fig. 1D). We observed even stronger defects in ventral muscle regions. In wild type, the ISNb defasciculates from the ISN and forms, among others, NMJs in the cleft between muscles 6/7 and on a ventral and medial position on muscles 12 and 13, respectively (Fig. 1E,F). In *piranha* mutants, we found that NMJs on muscle 12 and 13 were mislocalized or absent in 64.3 and 56.0% of hemisegments, respectively (Table 1, Fig. 1G). Muscles 6 and 7 showed an erroneous innervation pattern in 23.9 and 34.6% of hemisegments. It is important to note that the pattern and degree of misinnervation varied between hemisegments along the anterior-posterior axis and also between two hemisegments located on contralateral sides. We determined the total number of misinnervated muscles per hemisegment and found that between 7.1 and 46.4% of muscles were affected in *piranha* mutant hemisegments (n=84) compared with 0-14.3% in wild-type larvae (n=44). Thus, innervation errors occurred in all body wall regions and in every hemisegment, but the innervation pattern was unique for each hemisegment, indicating that the innervation process is largely autonomous within a given hemisegment.

As CD8-GFP-Sh is a transgenically encoded exogenous protein, it is possible that it does not accurately reflect the location of endogenous NMJs. To exclude this possibility, we stained *piranha* mutant larvae with antibodies that recognize synaptic marker

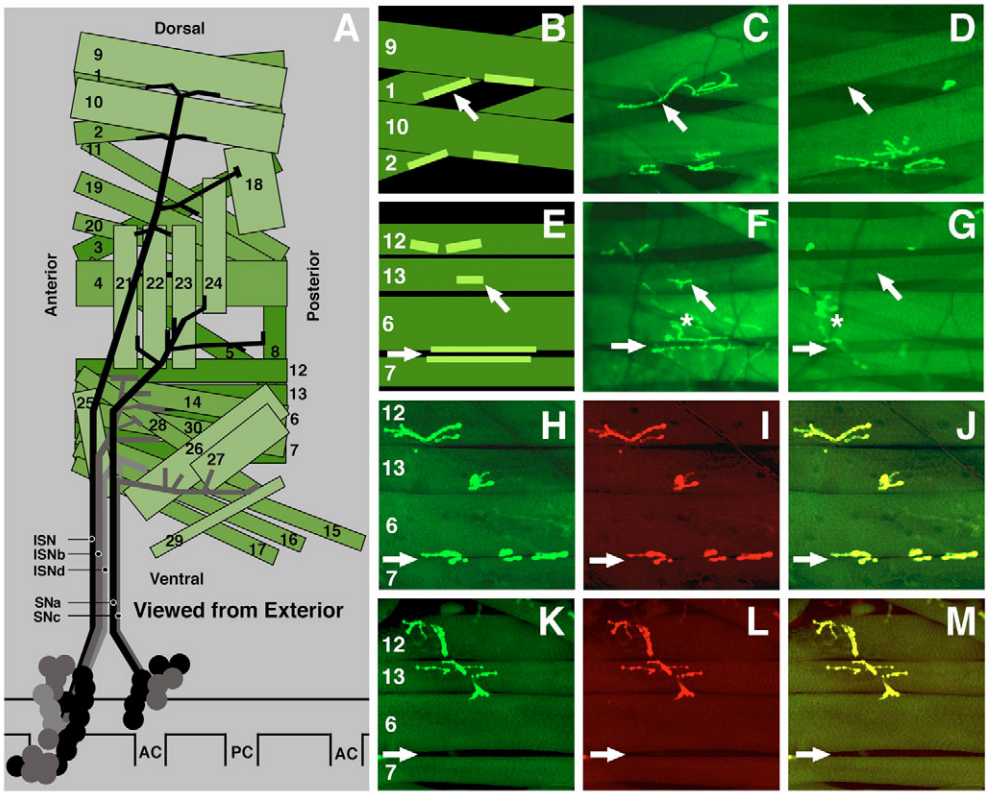

Fig. 1. Neuromuscular terminals are missing and mislocalized in *piranha* mutant third instar larvae. Arrows illustrate the normal localization of NMJs on muscles of wild-type larvae. (**A**) Schematic diagram of the innervation pattern of the somatic musculature of an abdominal hemisegment viewed from the exterior. The approximate branching pattern of the five motor nerves and the innervation sites are superimposed onto the muscle pattern. The approximate locations of motoneurons in the ventral nerve cord are indicated. (**B-D**) Innervation defects on dorsalmost muscles. (B) Schematic diagram and (C) confocal micrograph of NMJs (bright green) on muscle pairs 1/9 and 2/10 in undissected wild-type larvae as seen with the CD8-GFP-Sh marker (exterior view). (D) NMJs are missing on muscle 1 and reduced to a remnant on muscle 9 in this $piranha^{D427}/piranha^{K788}$ mutant hemisegment. (**E-G**) Innervation defects on ventral muscles. (E) Schematic diagram and (F) confocal micrograph depicting the locations of NMJs on ventral internal muscles 12, 13, 6 and 7 in an undissected wild-type larva expressing CD8-GFP-Sh. (G) In this $piranha^{D427}/piranha^{K788}$ mutant hemisegment, NMJs are missing on muscle 13 and rudimentary in the cleft of muscles 6/7. Muscle 12 displays innervation defects as well. Asterisks indicate NMJs and muscles outside of the intended focal plane. (**H-M**) Confocal images of the ventral innervation pattern of a dissected wild-type (H-J) and $piranha^{D427}/piranha^{K788}$ mutant larva (K-M) viewed from the interior. NMJs on muscles 12, 13, 6 and 7 are visualized with CD8-GFP-Sh (H,K) and anti-Dlg (I,L). Endogenous Dlg staining completely overlaps with transgenic CD8-GFP-Sh (J,M). Note the altered innervation pattern of muscles 12 and 13 and the lack of NMJs in the cleft between muscles 6 and 7 in the mutant animal (arrows in K-M). Dorsal is up and anterior is left in all figures. AC, anterior commissure; PC, posterior commissure.

proteins. Dlg is a postsynaptic protein that mediates the anchorage of transmembrane receptors to the underlying cytoskeleton (Budnik et al., 1996). We did not observe neuromuscular Dlg staining in places where CD8-GFP-Sh clusters were absent, neither in wild-type (Fig. 1H-J) nor in *piranha* mutant larvae (Fig. 1K-M). CD8-Sh-GFP therefore faithfully reflects the presence and positions of NMJs.

Misguided motor axons innervate muscles at ectopic locations in *piranha* mutants

As CD8-GFP-Sh visualizes only postsynaptic sides of NMJs but not motor nerves, we asked whether the unusual locations of NMJs in *piranha* mutants were caused by misguided axons. We stained dissected third instar larvae with anti-Fasciclin II antibodies (anti-Fas II). Fasciclin II is expressed by all motoneurons and accumulates

Table 1. Frequency of innervation errors in wild type, *tolloid-related 1* (*tlr1*, *piranha*) and *sidestep* (*side*) mutant animals

	ISN				SNa				ISNb				SNc			ISNd		
L3 larvae	M1	M9	M2	M10	M21	M22	M23	M24	M12	M13	M6	M7	M26	M27	M29	M15	M16	M17
Wild type (CD8-GFP-Sh) (*n*=44)	0	0	0	0	2.3	0	0	0	6.8	2.3	0	2.3	0	0	2.3	13.6	6.8	4.6
tlr^{D427}/tlr^{K788} (*n*=84)	38.1	25.0	7.1	3.6	8.4	1.2	1.2	34.5	64.3	56.0	23.9	34.6	21.7	74.7	71.1	83.4	27.4	34.6
$side^{C137}/side^{I1563}$ (*n*=60)	25.0	35.0	16.7	11.7	41.7	3.4	3.3	51.7	75.0	75.0	83.3	85.0	61.7	86.7	66.7	78.3	63.3	98.4
$tlr^{D427},side^{C137}/tlr^{K788},side^{C137}$ (*n*=65)	36.9	35.4	41.6	18.5	53.8	12.3	21.5	95.4	93.8	98.5	100	100	95.3	100	98.5	96.9	98.5	100

			ISNb bypass				
Stage 17 embryos	ISN defect	SNa defect	Fused full	Split full	Partial	SNc bypass	ISNd bypass
Wild type (CD8-GFP-Sh) (*n*=218)	1.4	2.8	0.9	1.8	3.7	1.8	14.7
tlr^{D427}/tlr^{K788} (*n*=211)	84.4	51.2	29.4	52.6	14.2	54.0	54.0
$side^{C137}$ (*n*=105)	14.3	22.9	36.2	15.2	32.4	67.6	65.7

(Top) Innervation defects in larvae. Numbers represent the percentage of hemisegments with innervation defects on the indicated muscles (mislocalized and missing NMJs) in third instar larvae stained with CD8-GFP-Sh. (Bottom) Innervation defects in embryos. Numbers represent percentage of hemisegments with guidance defects in the indicated motor nerves.
n, number of hemisegments quantified.

in their axons and presynaptic terminals, making it possible to selectively visualize motor nerves but not the afferent sensory nerves that project along similar pathways (van Vactor et al., 1993). In wild-type larvae, muscles 12 and 13 are innervated by a ventrodorsal projection of the ISNb pathway (Fig. 2A-C). In *piranha* mutants, we found that muscles 12 and 13 were often innervated via a dorsoventral projection of the ISN or SNa, which induced the formation of NMJs at ectopic sites (Fig. 2D-F). This suggests that motoneuronal growth cones of the ISNb pathway failed to navigate into the ventral muscle field via their normal route. Despite this initial failure, however, some growth cones eventually managed to detach from the ISN or SNa and innervated muscles 12 and 13 from the dorsal side (reach back phenotypes via a different nerve route). These experiments show that motor axons are misrouted in *piranha* mutants, which leads to the formation of synaptic terminals at ectopic locations.

During manual dissection of larvae, great care must be taken to preserve the trajectories of peripheral nerves. To circumvent this technical hurdle, we devised a genetic method that permits the visualization of both motor nerves and NMJs in living animals. Using the Gal4/UAS-system (Brand and Perrimon, 1993), we expressed the *Discosoma* Red Fluorescent Protein (UAS-dsRed2) specifically in motoneurons (OK371-Gal4) in the background of CD8-GFP-Sh wild-type or *piranha* mutant animals. Motor axons and presynaptic terminals were therefore highlighted in red and muscles and postsynaptic terminals in green (Fig. 2G-L). In wild-type larvae, the SN and ISN nerves form a single nerve bundle that defasciculates into five nerve branches at the ventralmost choice point (shown schematically in Fig. 2G). The ISNb and ISNd detach from the ISN, whereas the SNc detaches from the SNa (Fig. 2J). In *piranha* mutants, we observed that the ISNb frequently stayed attached to the ISN, sometimes as a separately identifiable axon bundle, and reached its target muscles via irregular routes (Fig. 2H,K). We found similar defasciculation errors in the SN pathway. As shown in Fig. 2I,L, the SN nerve often grew too far to the posterior, because the SNa defasciculates much too late. *piranha* mutant larvae display, therefore, severe bypass and misrouting phenotypes, primarily due to motor axons remaining attached to each other at choice points.

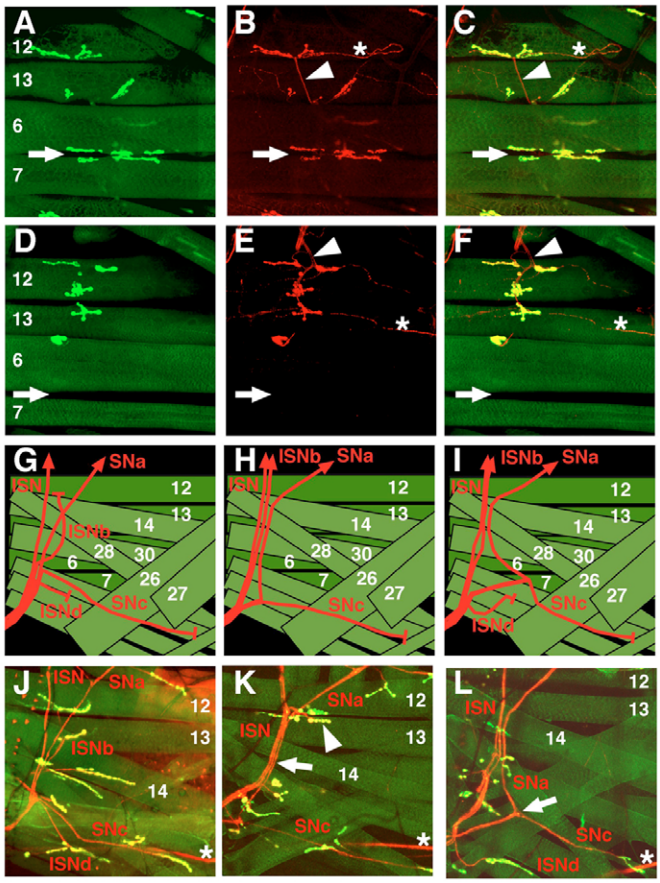

Fig. 2. Motor axons are misguided in *piranha*^{D427}/*piranha*^{K788} mutant larvae. (**A-F**) Confocal micrographs of the ISNb innervating ventral muscles 12, 13, 6 and 7 in dissected wild-type (A-C) and *piranha* mutant (D-F) larvae. Muscles and postsynaptic terminals are visualized with CD8-GFP-Sh (A,D), motor axons and presynaptic endings are stained with anti-Fasciclin II (B,E). The ISNb normally innervates muscle 12 on its ventral side via a ventrodorsal projection (arrowheads in B,C). In a *piranha* mutant hemisegment, muscles 12, 13 and 6 are innervated at ectopic sites by a dorsoventral nerve projection (arrowheads in E,F). Muscles 6 and 7 remain uninnervated (arrows in D-F). Arrows mark the cleft between muscles 6 and 7. Asterisks indicate type II boutons. (**G-L**) Transgenic labeling of motor axons reveals guidance defects in living *piranha*^{D427}/*piranha*^{K788} mutant larvae (exterior views). In addition to CD8-GFP-Sh, larvae express dsRed2 in all motoneurons using OK371-Gal4. (G,J) Schematic diagram (G) and confocal micrograph (J) of the hemisegmental nerve defasciculating into five nerve branches at the ventral choice point of a wild-type larva. (H,K) Schematic diagram (H) and confocal micrograph (K) of the defasciculation defects in a *piranha* mutant larva. The ISNb failed to branch into the ventral region and migrated in a parallel pathway along the ISN. The ISN, ISNb and SNa pathways are visible as separate nerve bundles (arrow). An axon branching out of the misguided ISNb innervates muscle 13 at an ectopic position (arrowhead). (I,L) Schematic diagram (I) and confocal micrograph (L) of the ventral muscle field of a *piranha* mutant larva. The SNa stays attached to the SNc and defasciculates too late (arrow). Asterisks in (J-L) indicate nerves innervating neighboring hemisegments.

Guidance errors in *piranha* mutants occur at embryonic stages

We asked next at which time point these projection errors develop, and we examined motoneuronal trajectories during stages 16-17 of embryonic development, when neuromuscular connectivity is established. The ISN of wild-type embryos has three clearly visible branch points (Fig. 3A). In *piranha* mutants, we observed in 84.4% of hemisegments (Table 1) that the branch points appeared underdeveloped and/or the ISN was stalled at the second branch point and barely reached the position of the third branch point (arrow in Fig. 3B). Within the developing SNa pathway, axons normally bifurcate into a dorsal and posterior branch at the dorsal edge of muscle 12 (Fig. 3C). In *piranha* mutant embryos, we found SNa defects in 51.2% of hemisegments, including, for example, two dorsal branches of the SNa (arrowheads in Fig. 3D). In ventral muscle regions, the ISNb failed to defasciculate from the ISN in 96.2% of hemisegments. The ISNb was either tightly attached to the ISN (fusion bypass, see left segment in Fig. 3D and Table 1) or formed a separated parallel nerve bundle (split bypass, middle and right segment in Fig. 3D and Table 1). In addition, we and others (M. Serpe and M. O'Connor, personal communication) observed defasciculation defects in Fasciclin II-positive nerve tracts in the embryonic central nervous system (data not shown). The innervation defects do not strongly compromise embryogenesis and larval development, because we recover *piranha*^{D427} mutant second and early third instar larvae at the expected ratios (data not shown).

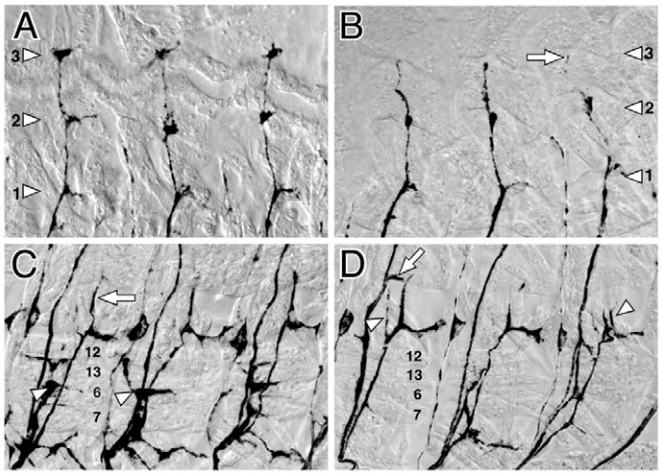

Fig. 3. Axon guidance defects in *piranha* mutants arise during embryonic development and affect all motor axon pathways. (**A-D**) Micrographs of motor axons in three consecutive hemisegments in dissected wild-type (A,C) and *piranha*^{D427}/*piranha*^{K788} mutant (B,D) embryos at stage 17 stained with anti-Fas II antibodies. (A) In the dorsal region of a wild-type embryo, the ISN has reached its terminal branch point at muscle pair 1/9 in all three hemisegments, and all three branch points are well developed (arrowheads 1-3). (B) The ISN fails to reach its final branch point properly (arrow) in *piranha* mutants, and most branch points appear underdeveloped (arrowheads 1-3). (C) Lateral and ventral body wall region of a wild-type embryo. The SNa bifurcates into a dorsal branch (arrow) and posterior branch. The ISNb (arrowheads) forms a clearly visible projection innervating muscles 12, 13, 6 and 7. (D) In *piranha* mutants, a bifurcated dorsal branch of the SNa is often observed (arrowheads). The ISNb fails to innervate muscles 12, 13, 6 and 7. In the left segment, the ISNb remains fused to the ISN and branches off at muscle 4 (arrow). In the middle and right segments, a split bypass occurs, with the ISNb temporarily detaching from the ISN (right) or fusing to different nerve tracts (middle).

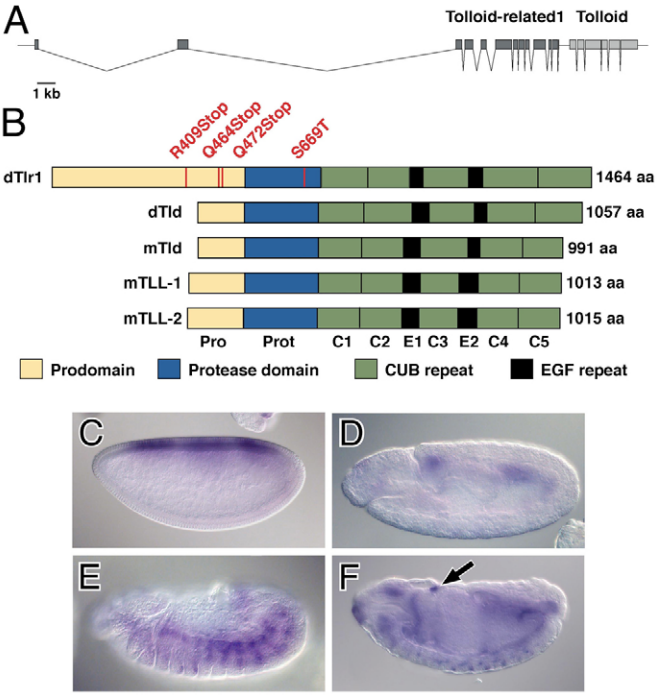

Fig. 4. Positional cloning of *piranha*. (**A**) Genomic organization of the *piranha* (*tolloid-related 1*, *tlr1*) locus. The 3′ end of the *tlr1* gene is less than 1 kb away from the 5′ end of its paralog *tolloid* (*tld*), limiting the 5′ regulatory region of *tld* to a minimum. (**B**) Domain structure of *Drosophila* Tlr1, Tld and their mouse homologs. The EMS-induced point mutations in the four *piranha* (*tlr1*) alleles are indicated (see text). (**C-F**) In situ hybridization using *tlr1* antisense probes. *tlr1* is expressed in the dorsal blastoderm at stage 5 (C), in progenitor cells of the visceral mesoderm at stage 10 (D), in somatic muscles at stage 13 (E) and in cells of the ventral nerve cord and ring gland (arrow) at stage 16 (F).

Based on these observations, we conclude that the *piranha* mutant guidance phenotype arises during embryogenesis, and the defects are quantitatively stronger but qualitatively similar to the larval defects.

Positional cloning of *piranha*

The *piranha* locus was mapped by meiotic recombination and deficiency mapping to the cytological region 96A2-A21 on the third chromosome. During meiotic mapping, we noticed homozygous mutant adult escapers that lacked the posterior crossvein of the wings. Literature and database searches revealed that mutants in *tlr1* [*tolkin* (*tok*)], located at 96A18-A19 (Fig. 4A), display a similar wing phenotype (Nguyen et al., 1994; Finelli et al., 1995). To examine if *piranha* is allelic to *tlr1,* we performed complementation crosses using existing *tlr1* alleles. Both *tlr1*^{1} and *tlr1*^{3} did not complement our *piranha* alleles, and the transheterozygous animals had both axon guidance and posterior crossvein defects. The *tlr1* cDNA encompasses 5.4 kb and encodes a predicted extracellular metalloprotease (Nguyen et al., 1994; Finelli et al., 1995). Consisting of 1464 amino acids, Tlr1 is composed of an N-terminal prodomain, a central metalloprotease domain and a C-terminal protein-protein interaction domain containing five CUB (complement subcomponents C1r/C1s, Uegf, BMP-1) and two EGF (epidermal growth factor) domains (Fig. 4B).

To identify potential molecular lesions, we sequenced the Tlr1-encoding exons and found single point mutations in all four *piranha* alleles. We therefore renamed our *piranha* alleles to *tlr1*^{K788}, *tlr1*^{D427}, *tlr1*^{K598} and *tlr1*^{I678}. Three of them contain nonsense mutations in the N-terminal prodomain: R409Stop in *tlr1*^{K788}, Q464Stop in *tlr*^{D427} and Q472Stop in *tlr1*^{K598} (Fig. 4B). Provided that the prodomain functions only in inhibiting the activity of the protease domain, these alleles are probably null alleles. Consistent with this assumption is the previous classification of *tlr1*^{1}, which contains a stop codon in the protease domain, as a null allele (Finelli et al., 1995). In the fourth allele, we identified a serine to threonine exchange within the protease domain (S669T in *tlr1*^{I678}). This highly conserved serine residue is located within the sequence motif ‘SIMHY’, which forms a characteristic loop, the Met-turn, that positions the terminal tyrosine residue to coordinate the zinc ion in the active site (Gomis-Ruth et al., 1993). Insufficient zinc coordination probably renders the protease domain non-functional in *tlr1*^{I678}. Indeed, a point mutation in the very same serine residue of the related metalloprotease Tolloid (S276F in *tolloid*^{10E}) has been isolated in a screen for new *tolloid* alleles (Finelli et al., 1994).

tolloid (*tld*) is a close sequence homolog and genomic neighbor of *tlr1*, with less than 1000 base pairs separating the two genes (Fig. 4A). Tolloid is involved in the determination of the dorsoventral body axis and functions as an activator of Decapentaplegic (Dpp) signaling in dorsal regions of blastoderm embryos (Shimell et al.,

1991; Marques et al., 1997). In mammals, four relatives of Tlr1 and Tld have been identified (Fig. 4B): mammalian Tolloid (Tld), bone morphogenetic protein 1 (Bmp1), Tolloid-like 1 (Tll1) and Tolloid-like 2 (Tll2), the first two of which are isoforms derived from the same gene (Takahara et al., 1994; Takahara et al., 1996; Scott et al., 1999). The metalloprotease domain of *Drosophila* Tlr1 is 64.5, 67.5 and 67.0% identical to its mouse relatives Tld, Tll1 and Tll2, respectively. The CUB/EGF protein-protein interaction domain is also well conserved and shows 42.0, 42.5 and 43.9% identity to these proteins.

To determine where *tlr1* is expressed during embryonic development, we synthesized Digoxigenin-labeled antisense probes using cDNA clone RH04849. *tlr1* showed a dynamic expression pattern during embryogenesis (Nguyen et al., 1994; Finelli et al., 1995). We observed *tlr1* expression first in the dorsal blastoderm (Fig. 4C). In the extended germ band stage, it was transcribed in progenitor cells of the visceral mesoderm (Fig. 4D). At stages 13-15, *tlr1* was expressed in somatic muscles and the midgut (Fig. 4E). Beginning with stage 15, *tlr1* transcripts also appeared in a few cells in the ventral nerve cord, the thoracic peripheral nervous system and the ring gland (Fig. 4F). Interestingly, *tlr1* was strongly expressed in muscles but not in neurons when motor axons leave the central nervous system, indicating that muscle-derived Tlr1 may be important for motor axon guidance.

Transgenic rescue experiments reveal that Tlr1 functions non-cell-autonomously

To determine in which tissue and during which developmental period Tlr1 is required, we performed transgenic rescue experiments using the Gal4/UAS system. We induced transcription of wild-type Tlr1 in a *tlr1* mutant background during different developmental stages using Heat shock-Gal4. Compared with wild-type animals (Fig. 5A), mutant animals transgenic for UAS-*tlr1* and Heat shock-Gal4 displayed strong innervation defects when reared at room temperature, because expression of Tlr1 is not induced (Fig. 5B). By contrast, mutant embryos that received a 1-hour heat shock (37°C) when they were 3-6, 6-9 or 9-12 hours old (stages 6-9, 10-12 or 12-15, respectively) developed into larvae with a normal innervation pattern (Fig. 5C). When we applied the heat shock at the end of embryogenesis (stage 17), however, we were unable to rescue the mislocalized NMJs in *tlr1* mutants, indicating that Tlr1 is ineffective after NMJs have formed. Hence, Tlr1 functions during mid- to late-embryonic stages, when neuromuscular connectivity is established.

To examine whether Tlr1 is required in nerves or muscles, we performed rescue experiments using tissue-specific Gal4-lines. As *tlr1* is strongly expressed in muscles during motor axon pathfinding, we reasoned that muscle-specific expression of Tlr1 might be sufficient for rescue. Indeed, expression of Tlr1 in all somatic muscles using G14-Gal4 completely restored the innervation pattern in homozygous mutant larvae (Fig. 5D). The rescued larvae were indistinguishable from wild-type animals with respect to the size and localization of their NMJs. Unexpectedly, however, expression of Tlr1 in all postmitotic neurons using Elav-Gal4 also completely restored the wild-type innervation pattern (Fig. 5E). When we expressed Tlr1 only in cholinergic neurons using Cha-Gal4, the mutant phenotype was not rescued, demonstrating that UAS-*tlr1* is not unspecifically expressed in the absence of a Gal4 driver (Fig. 5F). From these results, it appeared that Tlr1 could be expressed either in muscles or all neurons to fully rescue the guidance defects. As Tlr1 is likely to be a secreted protease, this finding could be explained by a non-cell-autonomous function of Tlr1. If secretion into the extracellular matrix or hemolymph is sufficient to deliver Tlr1 to the locations where its proteolytic activity is required, then expression of Tlr1 in tissues normally irrelevant for motor axon guidance should rescue the innervation defects. Using fat body-specific Pumpless-Gal4 (PPL-Gal4) or two different hemocyte-specific drivers (CG-Gal4 and Serpent-Gal4), we could completely restore the wild-type innervation pattern in *tlr1* mutants (data not shown), supporting a cell non-autonomous function for Tlr1.

To test whether Tlr1 is also sufficient to misdirect motor axons in a wild-type background, we overexpressed it either in the nervous system (Elav-Gal4) or in all muscles (G14-Gal4) but we did not observe any motor axon guidance phenotypes, as visualized with CD8-GFP-Sh (data not shown). We noticed, however, that overexpression of Tlr1 in wing discs (24B-Gal4) leads to a large central wing blister, suggesting that the function of Tlr1 during wing development is dosage sensitive: too little Tlr1 leads to missing posterior crossveins, whereas too much Tlr1 causes loss of adhesion between wing epithelia (data not shown).

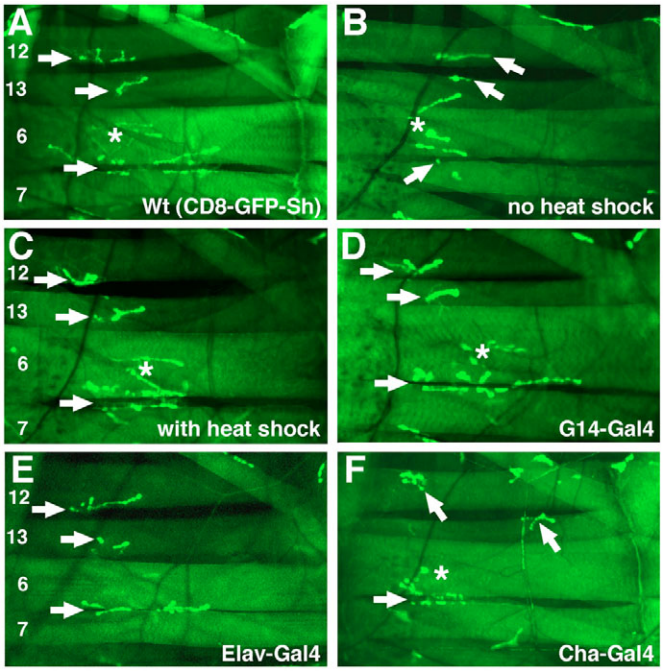

Fig. 5. The *tlr1* mutant phenotype can be rescued by expressing wild-type Tlr1 in various tissues. (**A-F**) Confocal micrographs of NMJs on ventral muscles 12, 13, 6 and 7 stained with CD8-GFP-Sh in undissected third instar larvae. Arrows indicate NMJs on muscles 12, 13, 6 and 7. (A) Wild type. (B) $tlr1^{D427}/tlr1^{K788}$ mutant larva carrying Heat shock-Gal4 and *UAS-tlr1* transgenes. When no heat shock is applied, the neuromuscular pattern is disrupted. Muscles 12 and 13 are innervated at wrong positions, and the cleft between muscles 6 and 7 is only marginally innervated (arrows). (C) Application of a heat shock during mid-embryogenesis completely rescues the innervation errors on all muscles. (D) Ventral muscle field of a $tlr1^{D427}/tlr1^{K788}$ mutant larva expressing Tlr1 in all somatic muscles using G14-Gal4. The innervation pattern appears wild-type. (E) Expression of Tlr1 in all postmitotic neurons using Elav-Gal4 similarly rescues the innervation errors in $tlr1^{D427}/tlr1^{K788}$ mutants. (F) The neuromuscular pattern is not restored in $tlr1^{D427}/tlr1^{K788}$ mutants expressing Tlr1 only in cholinergic neurons using Cha-Gal4. NMJs on muscles 12 and 13 are mislocalized (arrows). Asterisks indicate NMJs located on muscles that are outside the intended focal plane.

The metalloproteases Tolloid and Kuzbanian cannot functionally replace Tlr1

As mutations in *tlr1* affect a large subset, but not all, NMJs, we wondered whether the proteolytic activities of other metalloproteases are additionally required for pathway selection. As a closely related paralog of Tlr1, Tolloid may be required for the innervation of the remaining muscles. As strong alleles of *tld* are embryonic lethal, we searched for transheterozygous allelic combinations that would survive to third instar larvae. Compared with *tlr1* mutants (Fig. 6A), we were not able to detect mislocalized or structurally abnormal NMJs in tld^{6B69}/tld^{7074}, tld^{6B69}/tld^{9B66} or tld^{9B66}/tld^{10E95} mutants, indicating that Tolloid is not required for wiring and maintaining NMJs (Fig. 6B).

Both Tlr1 and Tld are members of the astacin family of metalloproteases, a subgroup of the metzincin superfamily, which comprises in addition the serralysins, the matrixins (matrix metalloproteases) and the adamlysins (ADAMs, metalloproteases with a disintegrin and metalloprotease domain) (Bond and Beynon, 1995; Stocker et al., 1995). Kuzbanian (Kuz), a member of the ADAM family in *Drosophila*, is expressed in neurons and has been shown to play a role in axon guidance at the ventral midline, raising the possibility that it may also regulate pathfinding of motor axons (Fambrough et al., 1996; Schimmelpfeng et al., 2001). When we examined kuz^{E29}/kuz^{K01403} mutant larvae, however, all NMJs were at their wild-type positions, indicating that motor axons project along correct trajectories (Fig. 6C). Other prime candidates for regulators of axonal pathfinding are matrix metalloproteases (Mmps). Mmps in general process extracellular matrix components, which is necessary for tissue remodeling and cell migration, but has also been shown to be crucial for axon guidance (Webber et al., 2002). *Drosophila* has only two Mmps, Mmp1 and Mmp2. During the time of motor axon pathfinding, Mmp1 is expressed in midline glial cells and Mmp2 in neurons and mesodermal cells, all tissues that are relevant for navigating growth cones (Llano et al., 2000; Llano et al., 2002; Page-McCaw et al., 2003). When we analyzed $Mmp1^{k04809}$, $Mmp2^{k00604}$ and $Mmp2^{KG01263}$ mutant larvae, however, we failed to detect any neuromuscular abnormalities (data not shown).

We next examined if Tlr1 and Tld could functionally replace each other if expressed in similar tissues. To test for functional redundancy, we crossed *UAS-tld* or UAS-*tlr1* into the *tlr1* mutant background and expressed either gene with Elav-Gal4 or 24B-Gal4. In contrast to experiments using *UAS-tlr1* (Fig. 6D), Tld was not able to substantially rescue the *tlr1* mutant phenotype, irrespective of whether we expressed it in neurons or muscles (Fig. 6E). Similarly, *UAS-kuz* failed to improve the projections errors in *tlr1* mutants (Fig. 6F), showing that neither Tld nor Kuz could functionally replace Tlr1. Thus, loss- and gain-of-function analysis of metalloproteases belonging to the matrixin, adamlysin and astacin families support a key-regulatory role of Tlr1 in motor axon guidance in *Drosophila*.

Axon guidance phenotypes are strongly enhanced in *tlr1,side* double mutants

To identify candidate molecules that might act in concert with Tlr1, we searched for mutants with related phenotypes. In our large-scale EMS mutagenesis screen of the larval NMJ, we identified four new alleles of *sidestep* ($side^{C137}$, $side^{I306}$, $side^{I1563}$, $side^{K717}$). Sidestep, originally identified by H. Sink and colleagues (Sink et al., 2001), is a transmembrane receptor of the immunoglobulin superfamily that functions as a muscle-derived attractant for motor axons. Similarly to *tlr1* mutants (Fig. 7A,7A'), we found missing and abnormally localized NMJs in $side^{C137}/side^{I1563}$ mutant larvae, regardless of whether we used CD8-GFP-Sh (Fig. 7B) or anti-Fas II antibodies (Fig. 7B') as detection methods. The immunohistochemical stainings also confirmed that the CD8-GFP-Sh marker reliably reflected the axon guidance defects in *side* mutants. In *side* mutant embryos, pathfinding of the ISNb was defective in 83.8% of hemisegments (Table 1). *tlr1* and *side* mutants therefore share a variety of phenotypic similarities: (1) embryonic defasciculation defects affect all pathways and persist into larval stages; (2) failures to reach final branch points; (3) innervation patterns vary between segments; (4) ventral muscles are more frequently affected; and (5) NMJs can be mislocalized or absent on an affected muscle fiber. For a majority of muscles, however, the *side* mutant phenotype was more penetrant (Fig. 7A'',B'').

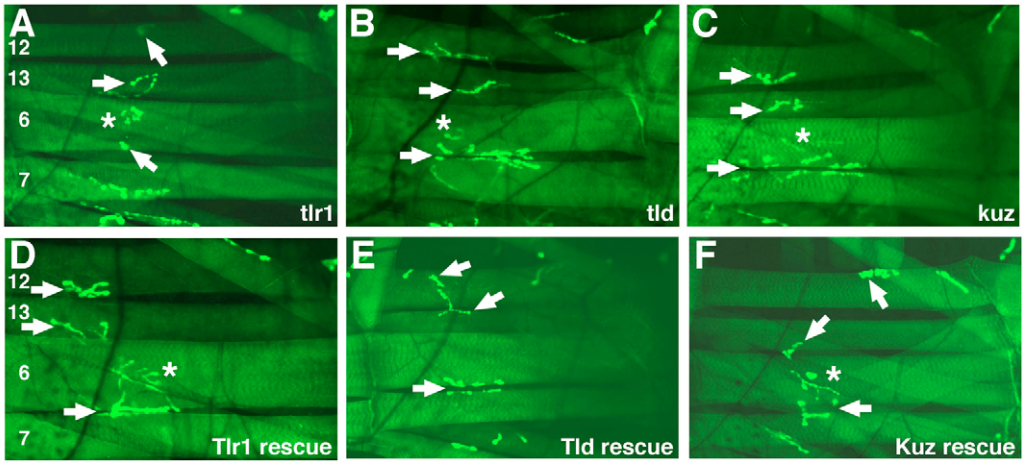

Fig. 6. Tolloid cannot functionally replace Tlr1. (**A-F**) Confocal images of the innervation patterns of ventral internal muscles in intact third instar larvae stained with CD8-GFP-Sh. Arrows indicate the locations of NMJs on muscles 12, 13, 6 and 7. (A) In a $tlr1^{D427}/tlr1^{K788}$ mutant animal, NMJs are mislocalized on muscle 12 and reduced to a remnant in the cleft of muscles 6 and 7. (B) All terminals are at their correct location and structured normally in a *tolloid* (tld^{10E95}/tld^{9B66}) mutant larva. (C) The neuromuscular innervation pattern appears wild-type in *kuzbanian* (kuz^{e29}/kuz^{K01403}) mutants. (D) Overexpression of Tlr1 in all neurons using Elav-Gal4 rescues the *tlr1* mutant phenotype. (E) Overexpression of Tld with Elav-Gal4 does not rescue the NMJ pattern in *tlr1* mutants. NMJs on muscles 12 and 13 are mislocalized in this hemisegment. (F) Overexpression of Kuzbanian in all neurons does not restore the innervation defects in *tlr1* mutants. NMJs are mislocalized on muscles 12 and almost absent on muscles 13, 6 and 7. Asterisks indicate NMJs located on muscles that are outside of the intended focal plane.

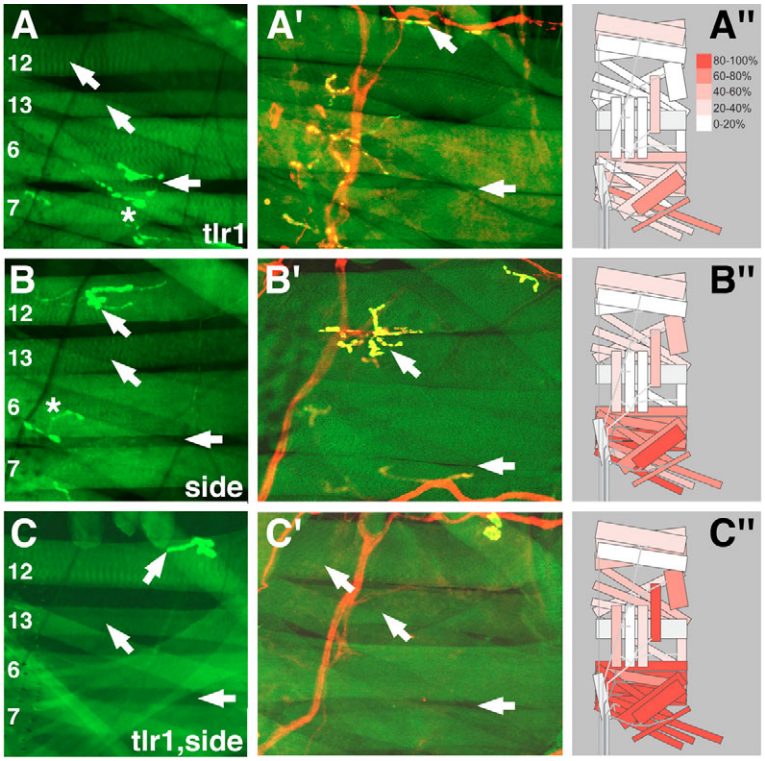

Fig. 7. Innervation defects are strongly enhanced in tlr1,side double mutants. Arrows indicate missing or mislocalized NMJs on muscles 12, 13, 6 and 7. Asterisks mark NMJs outside of the intended focal plane. (**A-C**) Confocal images of $tlr1^{D427}$ (A) and $side^{C137}/side^{l1563}$ (B) single and $tlr1^{D427},side^{C137}/tlr1^{K788},side^{C137}$ (C) double mutant third instar larvae stained with CD8-GFP-Sh. Double mutant larvae (C) show a strong enhancement of the innervation phenotype and lack almost all NMJs on ventral muscles, only muscle 12 is innervated at an unusual dorsal-posterior position in this example. (**A′-C′**) Confocal images of dissected $tlr1^{D427}/tlr1^{K788}$ (A′) and $side^{C137}/side^{l1563}$ (B′) single and $tlr1^{D427},side^{C137}/tlr1^{K788},side^{C137}$ (C′) double mutant third instar larvae stained with CD8-GFP-Sh (green) and anti-Fas II antibodies (red). In this double mutant hemisegment (C′), all NMJs are missing on ventral muscles, including NMJs formed by type II boutons. (**A″-C″**) Schematic representation of the quantitative evaluation of the larval innervation defects as presented in Table 1. The frequency of innervation errors for a respective muscle in wild type was subtracted from the frequency observed in mutants. Misinnervation frequencies were then transformed into a color code, as depicted in (A″). Muscles 4 and 25 were not evaluated. In tlr1 mutants (A″), the misinnervation phenotype is weaker than in side mutants (B″), and creation of a double mutant aggravates the innervation defects in ventral, lateral and dorsal body wall regions (C″).

As mutations in genes that function together in the same biological process often share phenotypic similarities, we created *side*,*tlr1* double mutants using genetic null alleles. If Tlr1 and Side function in a linear pathway, then double mutants would be predicted to exhibit a phenotype that resembles each single mutant phenotype. In $tlr1^{D427},side^{C137}/tlr1^{K788},side^{C137}$ double mutants, however, we observed a strong enhancement of each single mutant phenotype. Double mutant larvae lacked virtually all NMJs on all ventral muscles in all abdominal hemisegments (Fig. 7C,7C', Table 1). Muscles located in lateral or dorsal regions of the body wall also showed an increase in innervation errors, albeit less dramatically (Fig. 7C'', Table 1). The increase in phenotypic strength suggests that *tlr1* and *side* function in parallel pathways, or that their functions converge on shared components further downstream. Interestingly, *tlr1*,*side* double mutants were still capable of forming NMJs in lateral and dorsal regions, suggesting that additional gene products are involved in ensuring complete innervation of the musculature.

DISCUSSION

Motor axons are misrouted in *tlr1* mutants

In this paper, we show that *tlr1* is required for motor axons to defasciculate from other motor axons at specific choice points. *tlr1* encodes a secreted metalloprotease that functions non-cell-autonomously, possibly via secretion into the hemolymph. Mutations in *tlr1* lead to the permanent formation of NMJs at ectopic sites or to the absence of synaptic terminals. Only a few studies have examined whether embryonic motor axon guidance phenotypes persist into larval stages in *Drosophila* (Nose et al., 1994; Sink et al., 2001; de Jong et al., 2005). Apart from embryonic lethality, a possible reason is presumably that the detailed analysis of larval motor axon phenotypes is hampered by the availability of suitable methods other than manual dissection. We used transgenic methods for the visualization of the neuromuscular wiring pattern in intact larvae. The fluorescent CD8-GFP-Sh marker specifically highlights the postsynaptic apparatus of each muscle fiber, revealing the structure and location of each NMJ (Zito et al., 1999). As CD8-GFP-Sh is under the control of the myosin heavy chain promotor, we combined it with the Gal4/UAS-system to simultaneously express the red fluorescent protein dsRed2 in motoneurons. CD8-GFP-Sh by itself indirectly reflects the projection pattern of motor axons by reliably revealing the location of each NMJ. However, the combination of both CD8-GFP-Sh and motoneuron-specific dsRed2 highlights the entire neuromuscular connectivity pattern in living animals.

Supported by these non-invasive methods, we show that *tlr1* mutants have defects in motor axon guidance rather than in target recognition or innervation site selection. First, motor nerves show defasciculation defects already during embryogenesis, even before they reach their target muscles. Second, motor axons remain physically attached to each other beyond their destined branch points and until late larval stages. Third, the bypass, stall and misrouting phenotypes are similar to those found in *sidestep* mutants, a known regulator of motor axon guidance (Sink et al., 2001). As a result, motor axons fail to reach their targets in *tlr1* mutants or do so from unusual directions, which leads to anomalous muscle innervation. The formation of NMJs at ectopic locations suggests that the growth direction and entry point of the motor nerve may instruct the final location of an NMJ. Even if the position of an NMJ is predetermined by the muscle fiber, the incoming nerve terminal appears to be able to relocate postsynaptic components.

In *tlr1* mutants, all abdominal segments show innervation defects, and all pathways are affected. The intrasegmental phenotype, however, is quite variable, i.e. the innervation pattern of a given hemisegment differs visibly from the adjacent or contralateral hemisegment, indicating that neuromuscular wiring is largely autonomous for a given hemisegment. The variability further implies that Tlr1 may not regulate specific and invariable guidance decisions, but rather plays a general role in defasciculation.

Migrating growth cones in *tlr1* mutants apparently do not strictly rely on single molecular labels positioned at specific locations. These conclusions support the idea that exact target selection appears to be a rather stochastic process, in which the growth cones integrate attractive and repulsive cues provided by the microenvironment of surrounding cells (Winberg et al., 1998).

How does Tlr1 function?

Metalloproteases have been implicated in a variety of cellular processes, including cell migration, angiogenesis and metastasis (Sternlicht and Werb, 2001; Yong et al., 2001). Neuronal growth cones migrate through an environment that is rich in different extracellular surfaces and may thus exploit similar molecules and mechanisms as migrating cells. Despite the wealth of data on cell migration, only a few reports have been published implicating metalloproteases in axon outgrowth and guidance (Fambrough et al., 1996; Galko and Tessier-Lavigne, 2000; Hattori et al., 2000; Schimmelpfeng et al., 2001; Webber et al., 2002; McFarlane, 2003; Vaillant et al., 2003; VanSaun et al., 2003; Hehr et al., 2005; Jaworski et al., 2006). With regard to motor axons, only ADM-1 (*unc-71*), a member of the ADAM family in *Caenorhabditis elegans*, has been shown to regulate pathfinding (Huang et al., 2003). Tlr1 belongs to the astacin family of metalloproteases and is highly related to *Drosophila* Tolloid. Despite this high degree of conservation, we and others have shown that these two proteins have mutually exclusive functions (Nguyen et al., 1994; Serpe et al., 2005). While Tld cannot functionally replace Tlr1, it is still possible that other metalloproteases with redundant functions assist Tlr1 in defasciculation control, because not all guidance decisions are affected in *tlr1* mutants. Our loss- and gain-of-function analysis of related metalloproteases, however, did not support this possibility. In addition, no other metalloprotease has so far been recovered from mutant screens (van Vactor et al., 1993; Kraut et al., 2001; Sink et al., 2001). These observations support the idea that Tlr1 may be a key regulatory member of the metalloprotease family in *Drosophila* that controls motor axon guidance.

As a secreted metalloprotease, Tlr1 is predicted to function extracellularly, either in the extracellular matrix or in the interstitial fluid. Consistent with this prediction, overexpression of Tlr1 in hemocytes or cells of the fat body could fully rescue the *tlr1* mutant phenotype. Neither hemocytes nor fat-storing cells have so far been implicated in axon guidance. Hence, it is unlikely that Tlr1 remained associated with the extracellular matrix of these cells, but probably got released into the hemolymph. The circulating hemolymph then distributed it to where it was required. As endogenous Tlr1 is expressed in developing muscles during the period of axonal pathfinding, it is possibly secreted from there into the hemolymph to either proteolytically activate a repellent on motor nerves to induce defasciculation or to activate an attractant on muscles. The axon guidance receptor Sidestep is expressed on muscles and functions as an attractant for motor axons (Sink et al., 2001). Based on similarities in their loss-of-function phenotypes, Tlr1 could be required to activate the attractive function of Side. The phenotype of *tlr1,side* double mutants, however, was clearly stronger compared with each single mutant, indicating that they regulate the same biological process but that they function either independently or that the two functions converge further downstream. Tlr1 could therefore regulate the activity of an alternative pathway. Interestingly, M. O'Connor's group suggested that Tlr1 regulates motor axon guidance in part by activating latent TGF-β ligands (M. Serpe and M. O'Connor, unpublished). Although the exact molecular function of Tlr1 is currently not known, the data presented here clearly demonstrate that the evolutionarily conserved metalloprotease Tolloid-related 1 is necessary for motor axon guidance in *Drosophila*.

We are indebted to Mike O'Connor and Mihaela Serpe for sharing unpublished results. We also would like to thank Corey Goodman, in whose lab the EMS screen was performed, and Christiane Nüsslein-Volhard for support. We are grateful to Corey Goodmann, Mike O'Connor, Toshihiro Kitamoto, Rolf Reuter and Michael Pankratz for providing fly stocks and reagents. We thankfully appreciate the help of Dirk Beuchle for meiotic mapping, and Anne Spang and Matthew Harris for critically reading the manuscript. This project was funded by the Max-Planck Gesellschaft and the Deutsche Forschungsgemeinschaft (SFB446).

References

Aberle, H., Haghighi, A. P., Fetter, R. D., McCabe, B. D., Magalhaes, T. R. and Goodman, C. S. (2002). wishful thinking encodes a BMP type II receptor that regulates synaptic growth in Drosophila. *Neuron* **33**, 545-558.

Araujo, S. J. and Tear, G. (2003). Axon guidance mechanisms and molecules: lessons from invertebrates. *Nat. Rev. Neurosci.* **4**, 910-922.

Bond, J. S. and Beynon, R. J. (1995). The astacin family of metalloendopeptidases. *Protein Sci.* **4**, 1247-1261.

Brand, A. H. and Perrimon, N. (1993). Targeted gene expression as a means of altering cell fates and generating dominant phenotypes. *Development* **118**, 401-415.

Budnik, V., Koh, Y. H., Guan, B., Hartmann, B., Hough, C., Woods, D. and Gorczyca, M. (1996). Regulation of synapse structure and function by the Drosophila tumor suppressor gene dlg. *Neuron* **17**, 627-640.

de Jong, S., Cavallo, J. A., Rios, C. D., Dworak, H. A. and Sink, H. (2005). Target recognition and synaptogenesis by motor axons: responses to the sidestep protein. *Int. J. Dev. Neurosci.* **23**, 397-410.

Desai, C. J., Gindhart, J. G., Jr, Goldstein, L. S. and Zinn, K. (1996). Receptor tyrosine phosphatases are required for motor axon guidance in the Drosophila embryo. *Cell* **84**, 599-609.

Fambrough, D. and Goodman, C. S. (1996). The Drosophila beaten path gene encodes a novel secreted protein that regulates defasciculation at motor axon choice points. *Cell* **87**, 1049-1058.

Fambrough, D., Pan, D., Rubin, G. M. and Goodman, C. S. (1996). The cell surface metalloprotease/disintegrin Kuzbanian is required for axonal extension in Drosophila. *Proc. Natl. Acad. Sci. USA* **93**, 13233-13238.

Finelli, A. L., Bossie, C. A., Xie, T. and Padgett, R. W. (1994). Mutational analysis of the Drosophila tolloid gene, a human BMP-1 homolog. *Development* **120**, 861-870.

Finelli, A. L., Xie, T., Bossie, C. A., Blackman, R. K. and Padgett, R. W. (1995). The tolkin gene is a tolloid/BMP-1 homologue that is essential for Drosophila development. *Genetics* **141**, 271-281.

Galko, M. J. and Tessier-Lavigne, M. (2000). Function of an axonal chemoattractant modulated by metalloprotease activity. *Science* **289**, 1365-1367.

Gomis-Ruth, F. X., Stocker, W., Huber, R., Zwilling, R. and Bode, W. (1993). Refined 1.8 A X-ray crystal structure of astacin, a zinc-endopeptidase from the crayfish Astacus astacus L. Structure determination, refinement, molecular structure and comparison with thermolysin. *J. Mol. Biol.* **229**, 945-968.

Hattori, M., Osterfield, M. and Flanagan, J. G. (2000). Regulated cleavage of a contact-mediated axon repellent. *Science* **289**, 1360-1365.

Hehr, C. L., Hocking, J. C. and McFarlane, S. (2005). Matrix metalloproteinases are required for retinal ganglion cell axon guidance at select decision points. *Development* **132**, 3371-3379.

Hoang, B. and Chiba, A. (2001). Single-cell analysis of Drosophila larval neuromuscular synapses. *Dev. Biol.* **229**, 55-70.

Huang, X., Huang, P., Robinson, M. K., Stern, M. J. and Jin, Y. (2003). UNC-71, a disintegrin and metalloprotease (ADAM) protein, regulates motor axon guidance and sex myoblast migration in C. elegans. *Development* **130**, 3147-3161.

Jaworski, D. M., Soloway, P., Caterina, J. and Falls, W. A. (2006). Tissue inhibitor of metalloproteinase-2(TIMP-2)-deficient mice display motor deficits. *J. Neurobiol.* **66**, 82-94.

Kolodkin, A. L., Matthes, D. J. and Goodman, C. S. (1993). The semaphorin genes encode a family of transmembrane and secreted growth cone guidance molecules. *Cell* **75**, 1389-1399.

Kraut, R., Menon, K. and Zinn, K. (2001). A gain-of-function screen for genes controlling motor axon guidance and synaptogenesis in Drosophila. *Curr. Biol.* **11**, 417-430.

Krueger, N. X., Van Vactor, D., Wan, H. I., Gelbart, W. M., Goodman, C. S. and Saito, H. (1996). The transmembrane tyrosine phosphatase DLAR controls motor axon guidance in Drosophila. *Cell* **84**, 611-622.

Llano, E., Pendas, A. M., Aza-Blanc, P., Kornberg, T. B. and Lopez-Otin, C. (2000). Dm1-MMP, a matrix metalloproteinase from Drosophila with a potential

role in extracellular matrix remodeling during neural development. *J. Biol. Chem.* **275**, 35978-35985.
Llano, E., Adam, G., Pendas, A. M., Quesada, V., Sanchez, L. M., Santamaria, I., Noselli, S. and Lopez-Otin, C. (2002). Structural and enzymatic characterization of Drosophila Dm2-MMP, a membrane-bound matrix metalloproteinase with tissue-specific expression. *J. Biol. Chem.* **277**, 23321-23329.
Mahr, A. and Aberle, H. (2006). The expression pattern of the Drosophila vesicular glutamate transporter: A marker protein for motoneurons and glutamatergic centers in the brain. *Gene Expr. Patterns* **6**, 209-309.
Marques, G., Musacchio, M., Shimell, M. J., Wunnenberg-Stapleton, K., Cho, K. W. and O'Connor, M. B. (1997). Production of a DPP activity gradient in the early Drosophila embryo through the opposing actions of the SOG and TLD proteins. *Cell* **91**, 417-426.
McFarlane, S. (2003). Metalloproteases: carving out a role in axon guidance. *Neuron* **37**, 559-562.
Mitchell, K. J., Doyle, J. L., Serafini, T., Kennedy, T. E., Tessier-Lavigne, M., Goodman, C. S. and Dickson, B. J. (1996). Genetic analysis of Netrin genes in Drosophila: Netrins guide CNS commissural axons and peripheral motor axons. *Neuron* **17**, 203-215.
Nguyen, T., Jamal, J., Shimell, M. J., Arora, K. and O'Connor, M. B. (1994). Characterization of tolloid-related-1: a BMP-1-like product that is required during larval and pupal stages of Drosophila development. *Dev. Biol.* **166**, 569-586.
Nose, A., Takeichi, M. and Goodman, C. S. (1994). Ectopic expression of connectin reveals a repulsive function during growth cone guidance and synapse formation. *Neuron* **13**, 525-539.
Page-McCaw, A., Serano, J., Sante, J. M. and Rubin, G. M. (2003). Drosophila matrix metalloproteinases are required for tissue remodeling, but not embryonic development. *Dev. Cell* **4**, 95-106.
Parnas, D., Haghighi, A. P., Fetter, R. D., Kim, S. W. and Goodman, C. S. (2001). Regulation of postsynaptic structure and protein localization by the Rho-type guanine nucleotide exchange factor dPix. *Neuron* **32**, 415-424.
Salvaterra, P. M. and Kitamoto, T. (2001). Drosophila cholinergic neurons and processes visualized with Gal4/UAS-GFP. *Gene Expr. Patterns* **1**, 73-82.
Schimmelpfeng, K., Gogel, S. and Klämbt, C. (2001). The function of leak and kuzbanian during growth cone and cell migration. *Mech. Dev.* **106**, 25-36.
Scott, I. C., Blitz, I. L., Pappano, W. N., Imamura, Y., Clark, T. G., Steiglitz, B. M., Thomas, C. L., Maas, S. A., Takahara, K., Cho, K. W. et al. (1999). Mammalian BMP-1/Tolloid-related metalloproteinases, including novel family member mammalian Tolloid-like 2, have differential enzymatic activities and distributions of expression relevant to patterning and skeletogenesis. *Dev. Biol.* **213**, 283-300.
Serpe, M., Ralston, A., Blair, S. S. and O'Connor, M. B. (2005). Matching catalytic activity to developmental function: tolloid-related processes Sog in order to help specify the posterior crossvein in the Drosophila wing. *Development* **132**, 2645-2656.
Shimell, M. J., Ferguson, E. L., Childs, S. R. and O'Connor, M. B. (1991). The Drosophila dorsal-ventral patterning gene tolloid is related to human bone morphogenetic protein 1. *Cell* **67**, 469-481.
Sink, H. and Whitington, P. M. (1991). Location and connectivity of abdominal motoneurons in the embryo and larva of Drosophila melanogaster. *J. Neurobiol.* **22**, 298-311.
Sink, H., Rehm, E. J., Richstone, L., Bulls, Y. M. and Goodman, C. S. (2001). sidestep encodes a target-derived attractant essential for motor axon guidance in Drosophila. *Cell* **105**, 57-67.
Sternlicht, M. D. and Werb, Z. (2001). How matrix metalloproteinases regulate cell behavior. *Annu. Rev. Cell Dev. Biol.* **17**, 463-516.
Stocker, W., Grams, F., Baumann, U., Reinemer, P., Gomis-Ruth, F. X., McKay, D. B. and Bode, W. (1995). The metzincins-topological and sequential relations between the astacins, adamalysins, serralysins, and matrixins (collagenases) define a superfamily of zinc-peptidases. *Protein Sci.* **4**, 823-840.
Takahara, K., Lyons, G. E. and Greenspan, D. S. (1994). Bone morphogenetic protein-1 and a mammalian tolloid homologue (mTld) are encoded by alternatively spliced transcripts which are differentially expressed in some tissues. *J. Biol. Chem.* **269**, 32572-32578.
Takahara, K., Brevard, R., Hoffman, G. G., Suzuki, N. and Greenspan, D. S. (1996). Characterization of a novel gene product (mammalian tolloid-like) with high sequence similarity to mammalian tolloid/bone morphogenetic protein-1. *Genomics* **34**, 157-165.
Tautz, D. and Pfeifle, C. (1989). A non-radioactive in situ hybridization method for the localization of specific RNAs in Drosophila embryos reveals translational control of the segmentation gene hunchback. *Chromosoma* **98**, 81-85.
Tessier-Lavigne, M. and Goodman, C. S. (1996). The molecular biology of axon guidance. *Science* **274**, 1123-1133.
Vaillant, C., Meissirel, C., Mutin, M., Belin, M. F., Lund, L. R. and Thomasset, N. (2003). MMP-9 deficiency affects axonal outgrowth, migration, and apoptosis in the developing cerebellum. *Mol. Cell. Neurosci.* **24**, 395-408.
van Vactor, D., Sink, H., Fambrough, D., Tsoo, R. and Goodman, C. S. (1993). Genes that control neuromuscular specificity in Drosophila. *Cell* **73**, 1137-1153.
VanSaun, M., Herrera, A. A. and Werle, M. J. (2003). Structural alterations at the neuromuscular junctions of matrix metalloproteinase 3 null mutant mice. *J. Neurocytol.* **32**, 1129-1142.
Webber, C. A., Hocking, J. C., Yong, V. W., Stange, C. L. and McFarlane, S. (2002). Metalloproteases and guidance of retinal axons in the developing visual system. *J. Neurosci.* **22**, 8091-8100.
Winberg, M. L., Mitchell, K. J. and Goodman, C. S. (1998). Genetic analysis of the mechanisms controlling target selection: complementary and combinatorial functions of netrins, semaphorins, and IgCAMs. *Cell* **93**, 581-591.
Yong, V. W., Power, C., Forsyth, P. and Edwards, D. R. (2001). Metalloproteinases in biology and pathology of the nervous system. *Nat. Rev. Neurosci.* **2**, 502-511.
Zito, K., Parnas, D., Fetter, R. D., Isacoff, E. Y. and Goodman, C. S. (1999). Watching a synapse grow: noninvasive confocal imaging of synaptic growth in Drosophila. *Neuron* **22**, 719-729.